Evaluation of a commercial-grade camera for line field spectral-domain optical coherence tomography

Mathis Fauchart[a], Manuel J. Marques[a,*], Adrian Bradu[a], and Adrian Podoleanu[a]

[a]Applied Optics Group, School of Physical Sciences, University of Kent, Canterbury CT2 7NH, United Kingdom.
[*]M.J.Marques@kent.ac.uk

ABSTRACT

We investigate the utilization of a high frame rate, 2-D commercial-grade camera in a spectral domain (SD) OCT system driven by a super-luminescent (SLD) light source, using parallel illumination on the sample with a line focus (line-field SD-OCT, LF-SD-OCT). To this goal, several regimes of operation of the camera are evaluated, for different values of the exposure time, ISO and image size, assessing their suitability for depth resolved imaging. A-scans and B-scans of specular and scattering samples are produced, albeit of lesser quality than those we obtained in the past with a relatively expensive, high bit-depth, scientific camera. A comparative study involving several of the camera parameters and their impact on the system's imaging range and resolution is presented.

1. INTRODUCTION

In terms of speed and sensitivity, flying spot-based SD-OCT is the norm in ophthalmic imaging.[1] However, the costs of professional ophthalmic systems can still reach $150k.[2] Hence this study aimed at evaluating the possibility of using a commercial grade camera (<$0.5k) and full field line illumination to implement a SD-OCT system.

Full field imaging using 2D cameras was reported using swept source (SS)-OCT. Such configurations[3,4] are expensive due to the need of ultra-fast high bit rate cameras. Maintaining a 2D format for the camera but recurring to a broadband light source, then a compromise is achieved in terms of cost and functionality, where a single B-scan is produced, but the requirements in terms of the read-out rate of the 2D camera are more relaxed. This was first achieved by Nakamura *et al.*,[5] replicated using a 14-bit depth, scientific-grade camera by our group[6] and later further developed by Fechtig *et al.*[7] by employing an off-axis reference arm path, yielding high quality retinal images and demonstrating full axial range imaging.

In this communication, we report a line-field SD-OCT (LF-SD-OCT) system employing a high frame rate (up to 1,200 fps), commercial-grade camera in the spectrometer, and investigate the impact the acquisition parameters have on the system resolution and range. We also employ the Complex Master-Slave (CMS) method[8] to process the spectra. While we have reported CMS application to full-field OCT imaging,[9] this is the first report to use CMS in a line-field OCT system.

2. EXPERIMENTAL SET-UP

Figure 1 shows a sketch of the experimental set-up. A broadband super-luminescent diode (SLD) Superlum MS 371 is used, whose optical power is increased by a Superlum booster to 21 mW. The SLD central wavelength is 840 nm with a full bandwidth at half maximum (FWHM) of approximatively 50 nm. A line focus is created by a cylindrical lens (CL1, $f = 50\,\text{mm}$) at the entrance of the interferometer where the beam is split into two arms. A cylindrical lens (CL2, $f = 90\,\text{mm}$) is used to re-collimate the line created by the reflection on the mirror. On the object arm, a telescope is formed by two lenses, L1 and L2 ($f = 75\,\text{mm}$) to relay the line onto the sample behind a focusing lens L3 ($f = 25\,\text{mm}$). The back-scattered beam returned by the sample and the

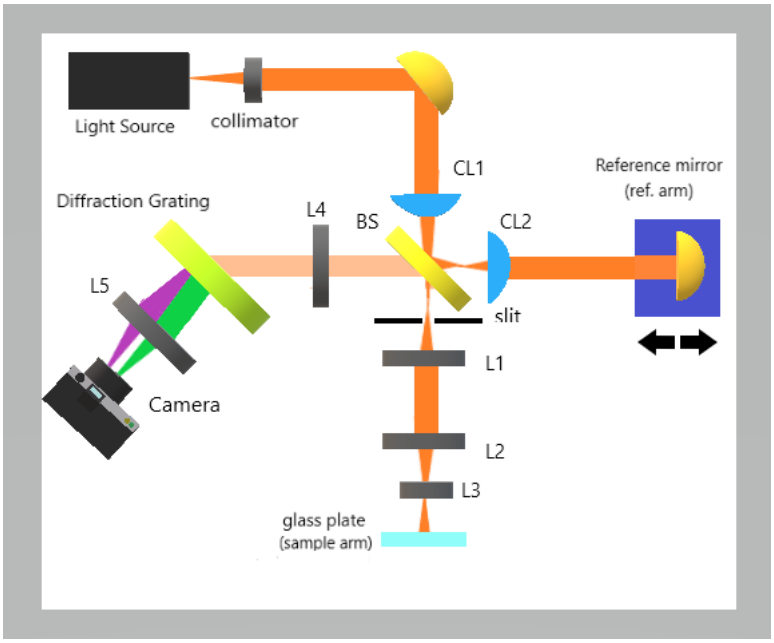

Figure 1. Experimental LF-SD-OCT set-up.

reference beam traverse lens L4 ($f = 75\,\text{mm}$) and are directed towards the diffraction grating. Finally, both signals interfere in the detector arm (L4, L5, $f = 75\,\text{mm}$). A diffraction grating (1800 lines/mm) and a lens L5 together with a 2D camera (Nikon 1 J5 model, sensor size: 13.2 x 8.8 mm, pixel pitch: $2.36\,\mu\text{m}$) constitute a spectrometer. The rows of the camera are along the horizontal direction of the sample while the columns are oriented along the spectral direction (vertical to the diagram plane in Fig 1). The reference mirror is mounted on a translation stage to adjust the optical path difference (OPD) in the interferometer.

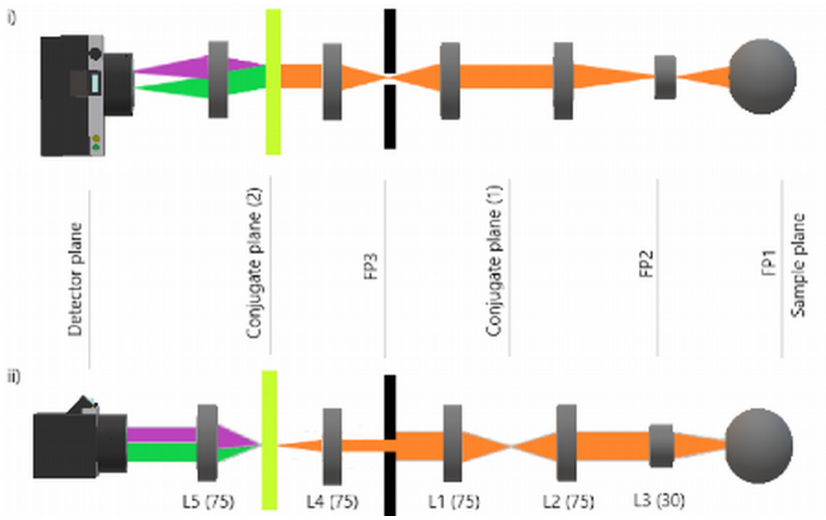

Figure 2. Vertical/Top view (i) and horizontal/side view (ii) of the ray propagation diagram through the system.

Figure 2 illustrates how the rays in vertical/top (i) and horizontal/side views (ii) propagate along the sample and spectrometer (detector) arms. It also represents the evolution of the beam size in 2D, where

the two telescopic arrangements (L1/L2 and L4/L5) are required to image the line from the sample in the camera sensor (i.e., the object plane and the detector plane are conjugated). The diffraction grating (in light green) spreads the various wavelengths in a plane parallel to the optical bench (two wavelength components are represented in Fig. 2 as green and purple beams).

The interference patterns are collected either as pictures or videos using the camera in different acquisition regimes, as detailed below. Files are transferred to a PC, where the spectral information is extracted and then processed using the Complex Master-Slave method.[8]

Initially, a mirror is used as a sample to calibrate the set-up. This consists of acquiring two images after placing the reference mirror at two different axial positions, generating two separate OPD values. After trimming these two interference patterns to keep the most relevant part (i.e. fringes), these two spectra are used to generate two functions that characterize the non-linearities in the spectrometer that chirp the fringes (make them non-periodic), g, and the dispersion in the interferometer, h. Also, a low pass filter is incorporated within the CMS code, during the calibration stage, to reduce the effects of the optical spectrum envelope in the calibration procedure. To increase the fringe contrast, the background is subtracted from the original pattern. This allows to minimize artifacts on the fringe pattern which might be caused by vibrations or undesired reflections by different optical components. Using functions g and h, a range of 100-1000 masks are software-generated to be used in the imaging process. After replacing the mirror in the sample arm with the actual sample being imaged, the spectral information in the images subsequently acquired by the camera can be compared against the software-generated masks, yielding a correctly represented B-scan with no need for further signal processing.

As previously mentioned, the camera we employed lets us work with different acquisition regimes: a manual, still picture mode and a video mode; both modes allowed the exposure time and ISO sensitivity to be varied, whereas the frame size could only be changed in the manual, still picture mode. Under these acquisition regimes, shots and videos were taken in a range of time from 62.5 μm to a few milliseconds. Higher exposure times would saturate the camera.

3. RESULTS AND DISCUSSION

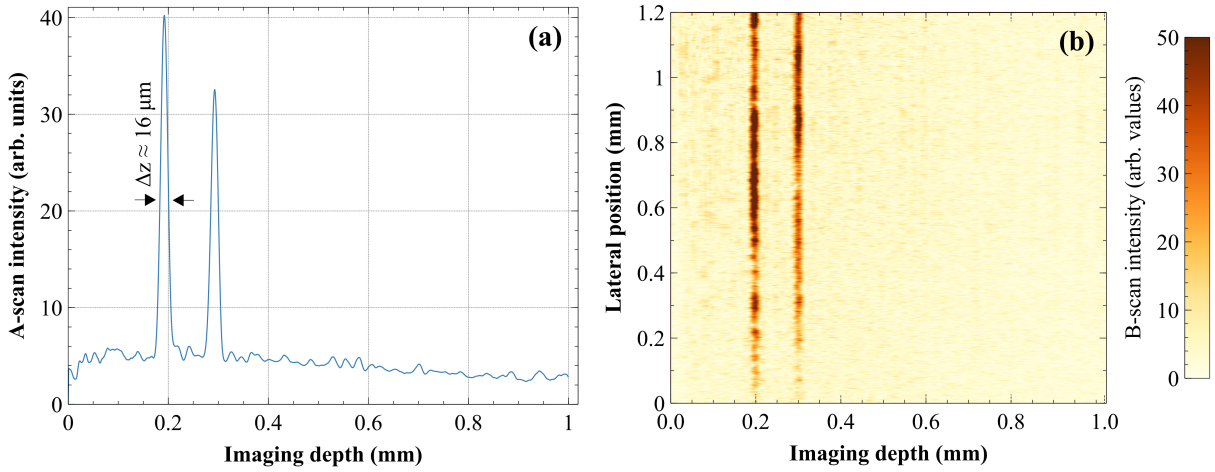

Figure 3. (a) A scan and (b) B-Scan from a microscope glass plate. Lateral and axial range of the B-scan are, respectively, 1.2 and 1.0 mm.

Using a glass phantom as a sample, an A-scan as shown in Fig. 3(a) display a full width at half maximum (FWHM) of the first peak of $\approx 16\,\mu$m. This is close to the value of the coherence-limited axial resolution of the system, which has been estimated to be $12.4\,\mu$m. The deviation can be explained by the camera sensor not covering the entire optical bandwidth and also due to spectral windowing (Hanning) being used to reduce the side-lobes in the A-scan peak.

By processing the entire 2-D image retrieved from the camera sensor, B-scan images from the sample are obtained (axial: 1024 pixels covering a range of 1 mm, lateral: 600 pixels covering approximately 1.2 mm on the sample). We can easily distinguish the two layers of the thin glass plate, as shown in Fig 3(b). The spacing between layers is ≈ 0.1 mm, and assuming a refractive index of 1.51 at $\lambda_0 = 840$ nm for the glass plate, its thickness is estimated as $70\,\mu$m, which roughly agrees with the manufacturer's specification of between 90 and $130\,\mu$m.

To assess the performance of the LF-SD-OCT system and optimize the operating parameters of the 2-D commercial-grade camera used, the Signal-to-Noise ratio (SNR) of the interference pattern produced with a single metallic mirror as sample was determined according to exposure time, ISO sensitivity and frame size settings on the camera.

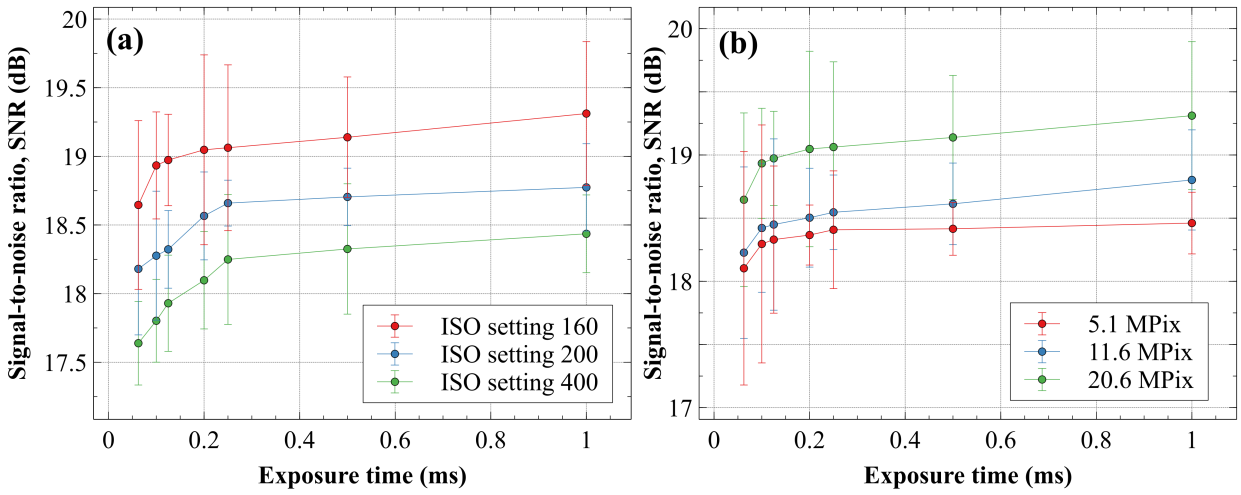

Figure 4. Both graphs illustrate the evolution of the SNR with the exposure time interval as a function of the ISO (left) and of the Image Size in megapixels (right). Image size was set to 20.6 MPix in (a) for all data sets and ISO was set to 160 in (b) for all data sets.

In Fig. 4, two plots are represented. Fig. 4(a) shows the effect of increasing exposure time (from 0.1 ms to 1 ms) on the SNR for several ISO settings, whereas Fig. 4(b) shows the same effect, but for several different frame sizes (in megapixels). The SNR measurements were averaged across the B-scan over 6 lateral points and the standard deviation plotted as error bars.

As expected, SNR increases when the exposure time increases. The fluctuations observed might be caused by the auto-focus mechanism from the camera, which introduces some noise. For Fig. 4(b), the fluctuations can also be derived from the selected lateral positions for the average, which could not be reliably maintained throughout the different data sets due to the changes in image size between data sets.

In Fig. 4(a), the SNR is higher for lower ISO sensitivity settings, which can be explained from the excessive background noise introduced at higher ISO settings. Reducing the number of pixels per frame seems to achieve the same effect; we conjecture that the camera is sub-sampling the pixels from the sensor rather than binning

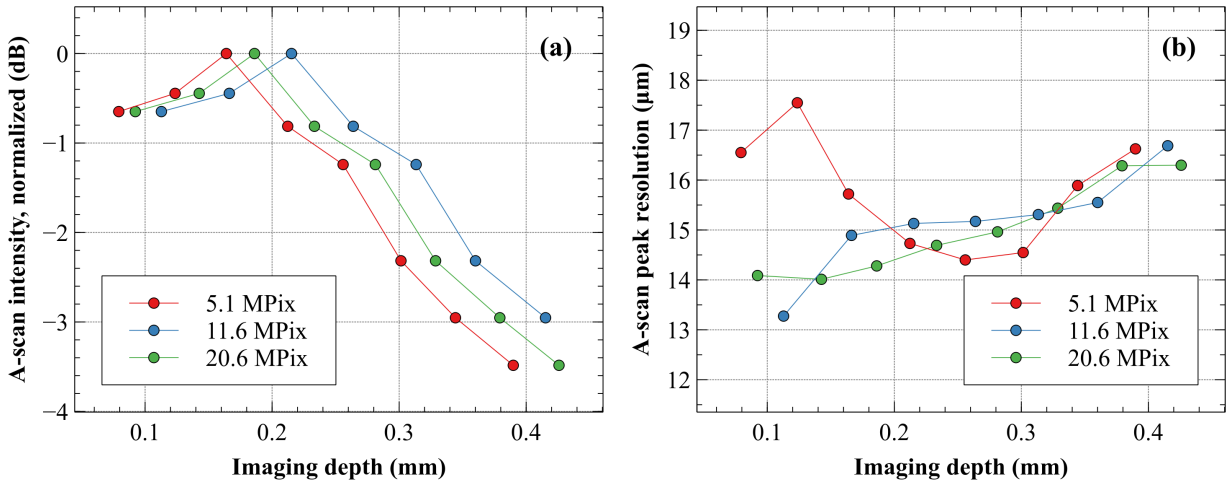

Figure 5. Comparison of the drop-off profiles (a) and axial resolution (b) for increasing imaging depths across various frame size settings. Across all data sets the ISO setting was kept at 160 and the exposure time was 0.2 ms.

them together, and this sub-sampling is occurring across the entire sensor, as no appreciable change was observed in the axial resolution, but a decrease in the axial range of the system was observed. This can be visualized in Figs. 5 (a) and (b).

In these two plots, we have assessed the visibility profile and axial resolution for several imaging depths over a range of roughly 0.4 mm, for several frame size settings. These measurements were taken by changing the position of the reference arm mirror (in steps of 0.05 mm) and acquiring CS at each position, while another mirror was kept in the focal position of L3 in the sample arm. A maximum attenuation of -3 dB is observed, consistent with the small imaging range studied; but more importantly, it is possible to detect a difference of 0.5 dB between different camera image size settings, with the lowest setting achieving the lowest performance, as expected. The axial resolution remained roughly constant across the interval at around $14 - 16\,\mu$m. For low depths, and low frame sizes (5.1 MPix), the gap observed for axial resolution might be due to non linearities or motion artifacts (eg. mechanical vibrations passed onto the system during acquisition) during image capture.

In conclusion, the study demonstrates the suitability of a commercial grade camera to perform OCT imaging when integrated in the spectrometer of a line-field OCT system. Camera settings, namely ISO, exposure time and image frame size, were varied to understand how they impact scanning spectra (A-scans) and 2D reconstructions of the sample (B-scans) through the OCT configuration, after a CMS application. Repeating the process for various configurations, and both camera regimes, we noticed that larger frame sizes (the maximum being 20.6 MPix) and lower ISO sensitivity (ISO 160) provide the highest quality interference patterns, and consequently higher SNR values. We have also established that the change in image frame size does not affect the axial resolution of the OCT system, although it does seem to impact the axial range by reducing the spectral resolution of the spectrometer.

ACKNOWLEDGMENTS

All authors acknowledge the European Research Council (ERC) ('ADASMART', 754695). M. Fauchart acknowledges the Erasmus+ programme, the University of Lille (France) and CROUS of Lille. M. J. Marques, A. Bradu and A. Podoleanu acknowledge the Engineering and Physical Sciences Research Council (EPSRC) ('REBOT', EP/N019229/1). A. Podoleanu acknowledges the National Institute for Health Research Biomedical

Research Centre at Moorfields Eye Hospital NHS Foundation Trust (NIHR), the UCL Institute of Ophthalmology, University College London, and the Royal Society Wolfson research merit award.

REFERENCES

[1] Drexler, W., Liu, M., Kumar, A., Kamali, T., Unterhuber, A., and Leitgeb, R. A., "Optical coherence tomography today: speed, contrast, and multimodality," *Journal of biomedical optics* **19**(7), 071412 (2014).

[2] Kim, S., Crose, M., Eldridge, W. J., Cox, B., Brown, W. J., and Wax, A., "Design and implementation of a low-cost, portable oct system," *Biomedical optics express* **9**(3), 1232–1243 (2018).

[3] Bonin, T., Franke, G., Hagen-Eggert, M., Koch, P., and Hüttmann, G., "In vivo Fourier-domain full-field OCT of the human retina with 1.5 million A-lines/s," *Optics letters* **35**(20), 3432–3434 (2010).

[4] Hillmann, D., Spahr, H., Pfäffle, C., Sudkamp, H., Franke, G., and Hüttmann, G., "In vivo optical imaging of physiological responses to photostimulation in human photoreceptors," *Proceedings of the National Academy of Sciences* **113**(46), 13138–13143 (2016).

[5] Nakamura, Y., Makita, S., Yamanari, M., Itoh, M., Yatagai, T., and Yasuno, Y., "High-speed three-dimensional human retinal imaging by line-field spectral domain optical coherence tomography," *Optics Express* **15**(12), 7103–7116 (2007).

[6] Wang, J., Dainty, C., and Podoleanu, A., "Line-field spectral domain optical coherence tomography using a 2D camera," in [*European Conference on Biomedical Optics*], 7372_21, Optical Society of America (2009).

[7] Fechtig, D. J., Grajciar, B., Schmoll, T., Blatter, C., Werkmeister, R. M., Drexler, W., and Leitgeb, R. A., "Line-field parallel swept source MHz OCT for structural and functional retinal imaging," *Biomedical optics express* **6**(3), 716–735 (2015).

[8] Rivet, S., Maria, M., Bradu, A., Feuchter, T., Leick, L., and Podoleanu, A., "Complex master slave interferometry," *Optics express* **24**(3), 2885–2904 (2016).

[9] Wang, J., Bradu, A., Dobre, G., and Podoleanu, A., "Full-field swept source master-slave optical coherence tomography," *IEEE Photonics Journal* **7**(4), 1–14 (2015).